Water Research 207 (2021) 117835

Contents lists available at ScienceDirect

Water Research

journal homepage: www.elsevier.com/locate/watres

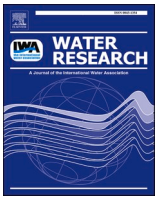

Rheological characterisation of alginate-like exopolymer gels crosslinked with calcium

N.M. Pfaff [a,d], J.A. Dijksman [b], A.J.B. Kemperman [c,d], M.C.M. van Loosdrecht [a,*], J.M. Kleijn [b]

[a] Department of Biotechnology, TU Delft, Van der Maasweg 9, HZ, Delft 2629, the Netherland
[b] Physical Chemistry and Soft Matter, Wageningen University, Stippeneng 4, WE, Wageningen 6708, the Netherland
[c] Membrane Science and Technology cluster, Faculty of Science and Technology, Mesa+ Institute for Nanotechnology, University of Twente, P.O. Box 217, AE, Enschede 7500, the Netherland
[d] Wetsus, European Center of Excellence for Sustainable Water Technology, Oostergoweg 9, MA, Leeuwarden 8911, the Netherland

A B S T R A C T

Bacterial alginate-like exopolymers (ALE) gels have been used in this work as a model for the extracellular polymeric matrix of biofilms. Aim was to relate the mechanical properties and strength of this matrix that make biofilms as persistent to cleaning as they are, to the complex cohesive molecular interactions involved. Mechanical properties of the gels as a function of $CaCO_3$ concentration were investigated using dynamic and static rheology. Gels with relatively low $CaCO_3$ concentrations, between 100 μmol and 300 μmol per g ALE, were found to exhibit similar viscoelastic behaviour as real biofilms, with elastic moduli between 50 Pa and 100 Pa and dissipation factors between 0.2 and 0.3. Increasing $CaCO_3$ concentrations resulted in an increase of the elastic modulus up to 250 Pa, accompanied by an increase in brittleness. At a $CaCO_3$ concentration of 1250 μmol per g ALE this trend stopped, probably due to disturbance of the continuous ALE network by precipitation of salts. Therefore, overdosing of Ca salts can be an adequate approach for the removal of biofouling. All gels exhibited permanent strain hardening under medium strain, and their mechanical properties showed dependency on their strain history. Even after application of an oscillatory strain with 200% amplitude that caused the gel structure to collapse, the gels recovered 65 to 90% of their original shear modulus, for the major part within the first 20 s. Recovery was slightly less for gels with high $CaCO_3$ concentration. In creep tests fitted with a Burgers model with multiple Kelvin elements at least three different interactions in the ALE gels could be distinguished with characteristic retardation times in the range of 10, 100 and 1000 s. Further identification of the mechanisms underlying the gel mechanics will allow the development of targeted strategies to undermine the mechanical strength of biofouling and aid the cleaning process.

1. Introduction

The complete chemical composition of biofilms is as diverse as the bacterial communities that inhabit them, and in most cases not easy to determine. Common practice is a distinction between two main components: the bacteria and the matrix of extracellular polymeric substances (EPS) (Geesey, 1982). Polysaccharides, proteins, lipids, nucleic acids and complex macromolecules with mixed functionalities have been identified in EPS (Seviour et al., 2019). These molecules form a physically crosslinked, 3D molecular network with the ability to bind high amounts of water. Therefore, biofilms can be considered as complex hydrogels. The EPS matrix, which can provide up to 90% of the biofilms' organic matter, acts as a protective shield for the bacteria against biological, chemical and mechanical influences. It also prevents desiccation. The EPS matrix has been shown to considerably reduce the effectiveness of biocides. Last but not least, the EPS matrix is responsible for the mechanical strength and integrity of biofilms.

The mechanical properties of biofilms have been found to stay mostly intact even if the bacterial cells are killed (Flemming, 2020). Therefore, the EPS matrix and its mechanical strength are essential in removing biofouling. Considering the biofilms' ability to resist physical forces, like the shear stress from flowing water, two aspects of the mechanical strength should be distinguished: the adhesion to the surface and the internal cohesion. The cohesion is reflected in the biofilms' viscoelasticity. Biofilms show the typical viscoelastic behaviour of crosslinked polymer networks (Safari et al., 2015). In contrast to covalently bound networks, the crosslinks in biofilms have for the most part been identified as physical interactions such as Vanderwaals forces, hydrogen bonds, electrostatic interactions including ion bridges, and entanglements (Seviour et al., 2019).

Cohesion and adhesion are closely related. Both follow from the molecular interactions within the EPS and with the environment. Especially for thin films, like many biofilms are, both properties can hardly be separated (Safari et al., 2015). Therefore, the influence of sample collection and treatment stays a relevant question in biofouling research. How does mechanical removal of biofilms from their

* Corresponding author.
E-mail address: M.C.M.vanLoosdrecht@tudelft.nl (M.C.M. van Loosdrecht).

https://doi.org/10.1016/j.watres.2021.117835
Received 6 September 2021; Received in revised form 31 October 2021; Accepted 1 November 2021
Available online 5 November 2021

substrates alter their physical characteristics? And how can the knowledge about such behaviour help to prevent and combat biofouling? These questions were the motivation for the current work. Goal is to relate the mechanical properties and strength of the EPS matrix to the molecular interactions involved in the dynamic crosslinks.

Alginate-like exopolymers' (ALEs) have been found to provide structural integrity to granular sludge and biofilms (Ghafoor et al., 2011; Lin et al., 2013). Therefore, we have chosen them as a model for the EPS matrix to investigate the mechanical properties of biofilms. Like the well-characterised algal alginate, this mixture of exopolymers forms gels with Ca^{2+} ions (Felz et al., 2016), which is important for adhesion and strength of biofilms containing ALE (Goode and Allen, 2011). Therefore, ALE provides an interim model between algal alginate and the complex, real-world biofilm EPS. In previous work (Pfaff et al., 2021), we have found that Ca^{2+} accumulates in thin ALE layers and influences their density. The current work focuses on the resulting cohesive strength of ALE gels as a function of Ca^{2+} content. The molecular interactions are probed by measuring the gels' time-dependant viscoelastic properties with a rheometer. The cohesion has been chosen over the adhesion to address the molecular interactions within the gels. To minimise the impact of adhesion, thick gel structures were produced and maximum adhesion (no slip) between the samples and the rheometer was ensured.

The swelling state of hydrogels has been found to impact mechanical strength, adhesion, permeability and degradation (Davidovich-Pinhas and Bianco-Peled, 2010). Inversely, the viscoelastic properties in combination with gel size and permeability have been found responsible for synaeresis (Scherer, 1989). Spontaneous synaeresis as a reaction to increasing salt concentrations in the supernatant has been described as a possibly important mechanism of biofilm survival during desiccation (Decho, 2016). Occurrence and peculiarity of synaeresis and its correlation with other characteristics was therefore a side focus of this work.

2. Materials and methods

2.1. ALE extraction

Because of the high ALE content of granular sludge, the material was extracted from Nereda® sludge collected from the wastewater treatment plant in Garmerwolde, the Netherlands. The extraction was done in alkaline conditions, followed by acid precipitation, based on a protocol by Felz et al. (2016).

The granules were collected by decantation. In 1 L demineralised water (purified with a MilliQ® IC 7003 system) ca. 150 g of the wet granules (20 g dry weight) were mixed with 10 g Na_2CO_3 (VWR, the Netherlands) and homogenised by pulsed sonication (Branson Sonifier 250, 5 min at 70%, max output 200 W). During sonication the mixture was cooled in an ice bath to prevent overheating. Subsequently, the alkaline extraction step was performed by heating the mixture to 80 °C for 30 min under vigorous stirring. The pellet was discarded after centrifugation (Allegra X-12R Centrifuge, Beckman Coulter, 20 min, 3750 rpm). The supernatant was dialysed in 4–6 steps using a Spectra/Por® Dialysis Membrane with a cut-off of 3.5 kDa, each against 20 L demineralised water until the conductivity in the dialysis solution was below 50 μS/cm. The extract was acidified with 1 M HCl (Merck Millipore, Germany) to pH 2 – 2.5. After another centrifugation the pellet was collected, lyophilised (ALPHA 2–4 LDplus, Christ, Germany) and stored at room temperature until further use. It is henceforth referred to as ALE (for further information we refer the reader to supplementary material C).

2.2. Gel preparation

Gels were prepared by internal gelation (Draget et al., 1989; Davidovich-Pinhas and Bianco-Peled, 2010), using $CaCO_3$ as a calcium source. Ca^{2+} ions were slowly released by hydrolysis of glucono-δ-lactone (GdL), enabling uniform gelling of the ALE. Based on the concentration ranges in which ALE films were found to be successfully formed on membranes (Pfaff et al., 2021), the concentrations were chosen as 40 g/L ALE and 5, 12.5, 25, 50 and 100 mm $CaCO_3$. An overview of the gels' composition is shown in Table 1. A molar ratio of 2:1 was applied between GdL and $CaCO_3$.

Stock solutions of ALE (50 g/L), $CaCO_3$ (10 × the target concentration shown in Table 1) and GdL (10 × target concentration) were prepared. The lyophilised ALE was dissolved in 1 M NaOH (Merck Millipore, Germany) and diluted with demineralised water. The solution was neutralised using more NaOH. $CaCO_3$ (anhydrous, reagent grade, VWR, the Netherlands) was suspended in demineralised water and dispersed in an ultrasonic bath (Bandelin, Sonorex Technik) for 10 min. GdL solutions were always freshly prepared by dissolving the necessary amount of glucono-δ-lactone (Sigma-Aldrich, France) in demineralised water. The three stock solutions were mixed in a volume ratio of 8:1:1. Portions of 1.5 mL were immediately pipetted into sandpaper (grit size P180, waterproof, Sencys, the Netherlands) lined disposable rheometer dishes (Anton Paar, 56 mm). The gel dimensions were determined by stencils of 30 mm diameter (see Fig. 1A). The samples were left for crosslinking at room temperature in a sealed plastic box partly filled with water, providing 100% humidity, for 36 h. Preliminary experiments showed that gelling was complete within this time frame.

Before starting the mechanical measurements, the stencils were removed, and the surfaces and heights of the gels were equalised by cutting them to 1 mm height using a 1 mm frame and a razor blade.

2.3. Gel sample analysis

2.3.1. Chemical characterisation

Crosslinked ALE-gel samples were scratched and weighed into dry porcelain crucibles (m_{sample}). After heating to 105 °C for 24 h, the dry mass (total suspended solids, *TSS*) was determined. The contained water, m_{water}, was calculated as the difference between m_{sample} and *TSS*. The dried samples were then burnt at 550 °C for 2 h to remove the organic matter (volatile suspended solids, *VSS*). The remaining ash was interpreted as the inorganic content of the material, while the *VSS* was interpreted as ALE. Eventually, the VSS density ρ_{VSS} was calculated as *VSS* per m_{water}.

2.3.2. Rheological measurements

Rheological characterisation of the samples was performed using an MCR 102 Rheometer (Anton Paar, Austria) with a 25 mm plate-plate geometry and disposable dishes (56 mm, Anton Paar, Austria) (cf. Fig. 1). The working principle of this apparatus is that samples are sheared between the upper rotating and the lower fixed plate while monitoring the displacement of the upper plate and the torque. A 3D-printed cover (PETG, printed with an Ultimaker S5, Ultimaker B.V., the Netherlands), of which the bottom part could be filled with water, was used to reduce evaporation of water during the measurements.

Before the start of every measurement, the upper plate was covered with clean sandpaper. The zero-height and measurement system inertia were recalibrated. The sample surface was detected by lowering the upper plate until a normal force of 0.15 N was reached. Corresponding to ca. 300 Pa, this is in the range of the expected moduli already, to make

Table 1
ALE, Ca^{2+} and gluconic acid content calculated for the gels from the initial sample compositions.

$CaCO_3$	ALE		Ca^{2+}		Gluconic acid	
[mm]	[g/L]	[wt%]	[g/L]	[wt%]	[g/L]	[wt%]
5	40	3.83	0.20	0.02	2.0	0.19
12.5	40	3.82	0.50	0.05	4.9	0.47
25	40	3.80	1.00	0.10	9.8	0.93
50	40	3.76	2.00	0.19	19.6	1.84
100	40	3.69	4.00	0.37	39.2	3.61

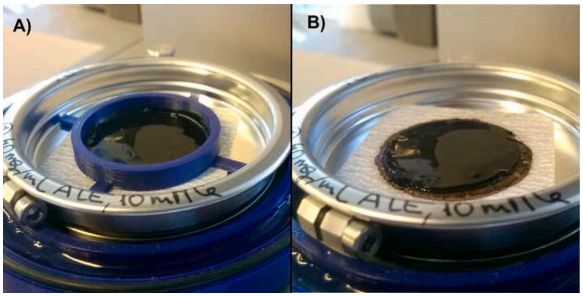

Fig. 1. ALE-gels were prepared in sandpaper lined disposable rheometer dishes. (A): preparation with a stencil, (B): sample after removing the stencil.

sure it was really the sample surface detected. Subsequently, the samples were trimmed and left equilibrating until the normal force remained below 0.05 N. Tests in the linear viscoelastic region (LVER), applying several of these approaching procedures with the sequence of slight compression and equilibration, resulted in identical measurements. The approaching procedure had no apparent impact on the results.

Amplitude sweeps. Oscillating measurements were performed in triplicates at 10 rad/s with exponentially increasing amplitudes between 0.01 and 250% shear strain (ε). The strain (deformation) was defined as the displacement in relation to the sample thickness. Measuring the resulting torque τ, the corresponding average shear stress σ on the sample was determined. The ratio between shear stress σ and shear strain ε is defined as the complex modulus G^*. Utilising the phase shift between σ and ε, the complex modulus G^* was split into the real component G', representing the storage modulus, and the imaginary component G'', representing the loss modulus. For a given strain, these moduli signify how much of the applied stress is stored elastically, and how much is lost by dissipation. The ratio between storage modulus G' and loss modulus G'' is also referred to as the dissipation factor tan δ. The so-called crossover point ($G' = G''$) can be used as a practical indicator for the dominance of viscous over elastic behaviour. It indicates that above the corresponding strain the network structure of a sample is broken. The strains and stresses at the crossover points were determined as a function of the $CaCO_3$ concentration.

Frequency sweeps. Frequency sweeps were performed with an amplitude of 0.3% strain (which was found to be inside the LVER in amplitude sweeps) with angular frequencies ω between 100 and 1 rad/s. More explanation and results can be found in the supplementary material B.

Recovery after oscillatory strain. The recovery capacity of the gels was investigated by observing the storage and loss moduli during application of different oscillatory strains at 10 rad/s. Again, all experiments were performed in triplicate. As reference and baseline a strain amplitude of 0.3% was used, which was well within the LVER. Strain amplitudes of 10, 30 and 200% were applied for 120 s each, followed by 400 s recovery at 0.3% strain.

Creep-recovery tests. Creep-recovery tests were performed in triplicate. A constant shear stress σ of 10 Pa, found to be inside the LVER for all samples, was applied for 300 s and the strain ε was monitored. Subsequently, the stress was removed and the strain was monitored for another 600 s.

The creep was interpreted using the Burgers model, which has been successfully applied to describe the viscoelastic behaviour of biofilms (Vinogradov et al., 2004). Because of creep ringing (the initial 'overshooting' visible in Fig. 2 at the first application of the stress, resulting from the coupling of instrument inertia and sample elasticity (Ewoldt and Mckinley, 2007), the first 5 s of each step were not included in the analysis.

In the current case an indefinite number of Kelvin elements was allowed. The ALE gels are described as a series of a Maxwell element, consisting of a spring (describing the elastic jump at the beginning of the curve), and a dashpot (describing the viscous response, represented by the linear increase at the end of the creep curve), and an indefinite number of Kelvin elements, consisting of a parallel spring-dashpot pairs (see Fig. 2). This results in the following equation:

$$\varepsilon_{creep}(t) = \frac{\sigma}{G_0} + \sum_n \frac{\sigma}{G_{K,n}} \cdot \left(1 - \exp\left(-t \cdot \frac{G_{K,n}}{\eta_{K,n}}\right)\right) + \frac{\sigma}{\eta_0} \cdot t \quad (1)$$

ε_{creep} is the shear strain measured over time t under application of a constant shear stress σ. G_0 is the initial elastic modulus, η_0 the viscosity, and $G_{K,n}$ and $\eta_{K,n}$ the elastic moduli and viscosities of each Kelvin element n.

The retardation time τ is a measure for the delay in the material's full elastic response to an applied stress, caused by its viscous elements. The characteristic retardation time τ of each Kelvin element is represented by the ratio between the viscosity and the elastic modulus. It depicts the time after which 63% of the maximum strain of the element is reached:

$$\tau_{K,n} = \frac{\eta_{K,n}}{G_{K,n}} \quad (2)$$

Similarly, for a simple Maxwell liquid the characteristic relaxation time is given by

$$\tau_M = \frac{\eta_0}{G_0} \quad (3)$$

Also for materials with a stress relaxation that is more complicated,

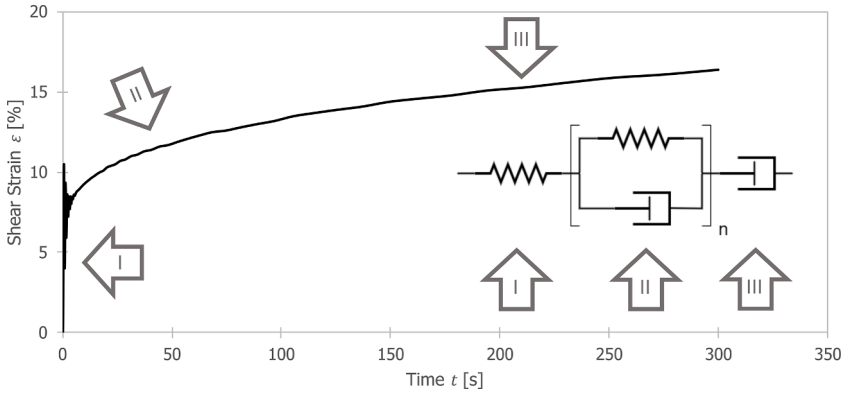

Fig. 2. *Analysis of a creep step*. The mechanical analogy to the ALE's behaviour is shown, according to the Burgers model with multiple Kelvin elements: the initial jump upon application of the stress is depicted by an elastic spring (I), while the steady incline towards the end is described by a dashpot (III). The intermediate curvature can be described by n pairs of parallel springs and dashpots (II).

like the investigated case, this equation is a reasonable estimate, with τ_M representing the longest retardation time in the system.

3. Results and discussion

3.1. Swelling and synaeresis over gelation

The ALE gels were prepared with equal amounts of ALE, but different amounts of $CaCO_3$ and glucono-δ-lactone (GdL). GdL hydrolyses in water forming gluconic acid, which adds to the final VSS.

Table 1 shows the composition of the samples at the beginning of the gelling process.

The ALE gels were left for gelling in a 100% humidity environment to avoid evaporation. It can be observed in

Fig. 3 that the final gel composition differed from the original sample composition. Salts have been neglected in this observation because they provide only 0.5 wt% (cf.

Table 1). Only at 5 mm $CaCO_3$ the original composition was almost maintained. With increasing Ca^{2+}:ALE ratio, the VSS density and thus the ratio of VVS to water increased (cf. also Fig. A1 in the supplementary material A). Apparently, during gelation water was expelled from the samples. This phenomenon is known as synaeresis and has been described for several hydrogel systems, including Ca-alginate (Kuo and Ma, 2001). Synaeresis is essentially a contraction of the hydrogel network resulting from molecular interactions within. The ALE network is getting compacter with increasing $CaCO_3$ concentration.

ALE densities of the gels were found between 45 and 70 g/L, in good agreement with those found for ALE gel layers produced in dead-end filtration with $CaCl_2$ (Pfaff et al., 2021). The common explanation for the observed compaction (up to a maximum at 50 mm $CaCO_3$) is a higher number of crosslinks. However, the amount of negative charges in the ALE has previously been estimated around 1 mmol/g VSS (Pfaff et al., 2021), corresponding to 40 mmol/L in the gels. Assuming that two negative charges are necessary for neutralisation of each Ca^{2+} ion, this means that the maximum amount of bound Ca^{2+} would be 20 mM. Therefore, other explanations considering internal restructuring processes like lateral association of the present crosslinks (Hermansson et al., 2016) seem worthwhile to consider.

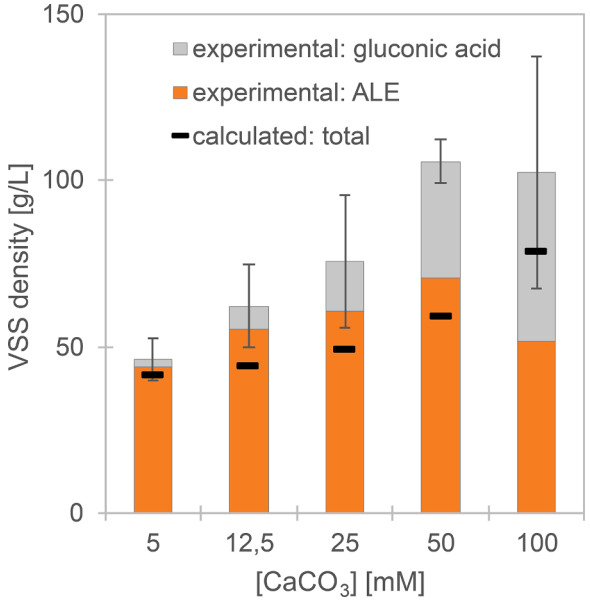

Fig. 3. VSS density inside the ALE gels. The experimentally determined values, shown as bars, are split into the contribution from ALE and gluconic acid. The error bars depict the statistical error in the total VSS content. In addition, the values as calculated from the composition before gelling are presented as black beams.

Concerning the influence of the gluconic acid, it can be assumed that the monomeric sugar does not form a network by itself, but rather dissolves in the water phase of the gels. Possible direct interactions with the ALE network are beyond the scope of this work. The solubility of calcium gluconate is 35 g/L at 25 °C (International Labour Organization, 2009), defining a solubility product of 2.15×10^3 mol^3/L^3. This value is only reached for the ALE gels with 50 mm and 100 mm $CaCO_3$. At 100 mm $CaCO_3$, gluconic acid represented almost 50% of the VSS and is available for recombination with calcium. For $CaCO_3$, the solubility is only 14 mg/L at 25 °C (International Labour Organization, 2012), corresponding to a solubility product of 1.96×10^{-2} $mmol^2/L^2$. This is already exceeded for ALE gels with 25 mm $CaCO_3$. At 50 mm $CaCO_3$, already more than half of the added calcium is probably present as precipitate. It is considered probable that the precipitation of calcium salts affects the structural homogeneity of the ALE gels. This may explain the decreasing density of the ALE network at very high concentrations. As shown in

Fig. 3, the standard deviation in VVS density of the 100 mm $CaCO_3$ gels was too large to draw definite conclusions. Also for the following discussions, the results on the 100 mm $CaCO_3$ gels were therefore not used for drawing conclusions on the behaviour of ALE gels as a model for biofilms. Nonetheless, we present these results since they have the potential to illustrate the effect of salt precipitation on the observed trends.

3.2. Viscoelastic behaviour

A representative example of an amplitude sweep is shown in Fig. 4. It can be seen that at lower shear strains ε, up to ca 10%, the moduli were independent of the applied strain and stress. This region is referred to as the linear viscoelastic region (LVER), where no permanent damage is done to the structure of the sample. It was defined as the region where the modulus values did not differ more than 5% from the average. In contrast, the crossover point was used as an indication for the destruction of the gel's network structure.

The storage modulus was the predominant factor in the LVER for all analysed samples. In Fig. 5 the storage moduli and dissipation factors in the linear elastic region are plotted as a function of the calcium concentration. The course of the storage modulus G' (A) was fairly similar to that of the VSS density (cf.

Fig. 3). It increased with the calcium concentration up to 50 mm Ca^{2+}, corresponding to a ratio of 1.25 mmol Ca^{2+} per g ALE. Above this

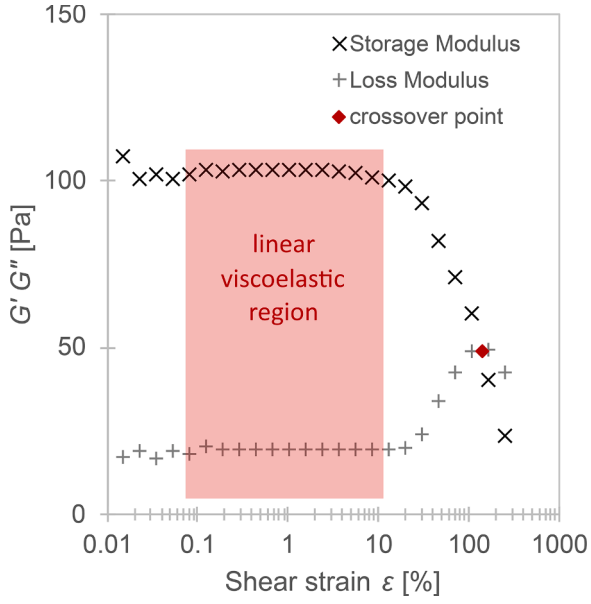

Fig. 4. Typical amplitude sweep for a 40 mg/L ALE, 12.5 mm $CaCO_3$ gel. The linear viscoelastic region and the crossover point are highlighted.

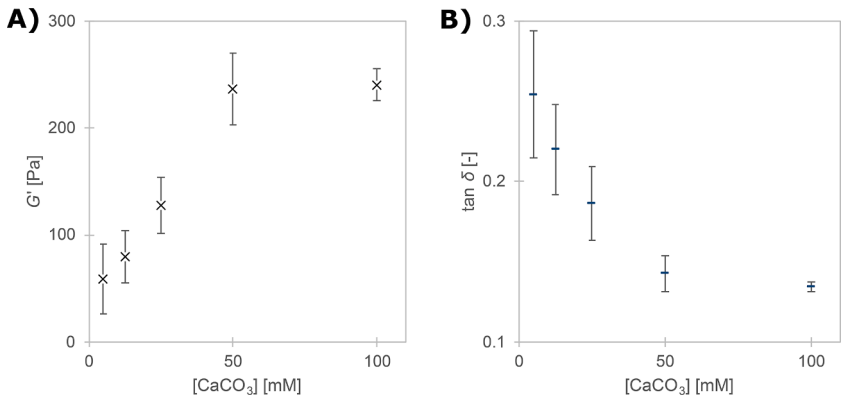

Fig. 5. Storage moduli G' and dissipation factors tan δ extracted from amplitude sweeps of ALE gels as a function of calcium concentration. The error bars show the standard deviation over the performed triplicates.

concentration, a further increase in calcium did not result in a further increase of *G'*.

The observed positive correlation of the elastic modulus with calcium concentration corresponds with expectations and with observations on biofilms (Körstgens et al., 2001). The apparent upper limit of this correlation could be a sign for oversaturation of $CaCO_3$, as discussed above. For Ca-alginate gels, oversaturation of calcium has been found, resulting in the formation of calcium precipitates that were correlated with a slight weakening of the gels (Kuo and Ma, 2001).

The maximum storage modulus for 40 mg/L ALE gels was found to be around 250 Pa (Fig. 5A). The dissipation factor was found to be between 0.3 and 0.15 (Fig. 5B). With increasing calcium content the domination of the elastic energy storage increased. This trend flattened out above 50 mm $CaCO_3$.

Apparently, at lower Ca^{2+} levels, the same interactions that caused an increase of the elastic modulus (e.g. an increasing number of cross-links) also resulted in contraction of the network, causing liquid to be pressed out. In the current work, synaeresis is less pronounced at low (5–10 mm) Ca^{2+} concentrations with dissipation factors above 0.2. The viscoelastic data obtained for these gels correspond well with results from the few available rheological experiments on intact biofilms (Vinogradov et al., 2004; Patsios et al., 2015).

3.2.1. *Response to constant shear stress*

Frequency sweeps showed that, if left alone, the ALE gels keep their elastic characteristic at least in the time frame of minutes (see also supplementary material B). In most applications, however, biofilms are exposed to continuous forces. An example is the shear force exerted by the water flow over a membrane. The effect of such forces was investigated with creep tests. All recorded creep curves followed the concave shape presented in Fig. 2, indicating viscoelasticity and the absence of ruptures. The creep-strain data over time was fitted according to Eq. (1). The use of two Kelvin elements ($n = 2$) was found to be sufficient to fit all measurements. This choice was based on the magnitude and even distribution (no visible trends) of the residuals (cf. inset of Fig. 6). In Fig. 6a representative creep experiment with the corresponding Burgers fit is shown. While all data points are plotted, only those above 5 s were considered for the fit to avoid disturbance by creep ringing. Datasets containing the Maxwell elastic modulus (G_0) and viscosity (η_0) as well as the elastic moduli ($G_{K,1}$, $G_{K,2}$) and viscosities ($\eta_{K,1}$, $\eta_{K,2}$) of the Kelvin elements were derived (cf. Eq. (1). The latter ones were combined into the characteristic retardation times according to Eqs. (2 and (3).

The Maxwell elastic moduli (supplementary material, Fig. A2-A) were in good agreement with the storage moduli from the amplitude sweeps (Fig. 5). The viscosity was found following the same trend, increasing with calcium concentration (supplementary material, Fig. A2-B).

In Table 2 the characteristic retardation times extracted for the two Kelvin elements are shown as well as the estimated Maxwell retardation time. They were found all to be rather unaffected by changes in the Ca^{2+} concentration, and in the order of 10, 100 and 1000 s, respectively. Rather than depending on the Ca^{2+} concentration or strain, these

Table 2
Characteristic retardation times τ of the different ALE gels, derived from creep experiments.

	$\tau_{k,1}$ [s]	$\tau_{k,2}$ [s]	τ_M [s]
5 mm $CaCO_3$	12.3 ± 0.6	82.3 ± 4.1	1144 ± 22
12.5 mm $CaCO_3$	11.2 ± 0.7	85.2 ± 6.2	1203 ± 292
25 mm $CaCO_3$	12.2 ± 1.0	74.2 ± 11.7	950 ± 116
50 mm $CaCO_3$	10.8 ± 0.3	77.3 ± 3.2	901 ± 123
100 mm $CaCO_3$	6.3 ± 5.1	65.2 ± 19.3	741 ± 321

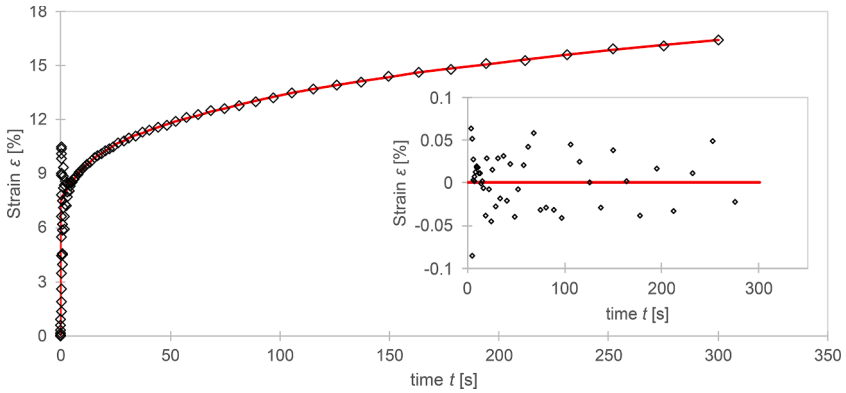

Fig. 6. Experimental creep data and Burgers fit with two Kelvin elements of an ALE gel containing 25 mm Ca^{2+}. The inset shows the deviation of the data from the fit.

characteristic times are only dependant on the type of interactions involved (Ehret and Böl, 2013). They are interpreted as a lifetime of those interactions (Grindy et al., 2015).

In Fig. 7 the change in strain over time is compared for the creep and recovery steps of ALE gels with 5 mm Ca^{2+} (A) and with 25 mm Ca^{2+} (B). It can be clearly observed that with the same stress a much larger strain is obtained in the gels with lower Ca^{2+} content, illustrating the different storage moduli (cf. Fig. 5). Also differences in the recovery of the strain are visible. While in the 5 mm experiment the recovery strain graph obviously differs from the creep graph from the beginning, in case of the 25 mm experiment they appear identical up to ca. 30 s. The final recovery of the strain was found between 80 and 90% (see Table A1 in supplementary material). This is in line with the results of the Burgers fits of the creep data, showing that the viscous contribution to the deformation, i.e. the non-recoverable part, is between 13 and 18%.

The molecular interpretation of these findings is based on considering the gels as a polymeric network, reversibly crosslinked via physical interactions, in particular Vanderwaals forces, hydrogen bonds, electrostatic interactions and entanglements. The property of behaving like a liquid on a longer time scale has been attributed to a limited life-span of all of these interactions in a network exposed to stress or strain (Ehret and Böl, 2013). This means that a particular bond in the gel may stay intact during a short exposure to stress, but breaks and potentially rearranges in another place when the exposure continues over a longer period. In the case of the ALE gels tested in this work, four different regimes have been distinguished:

- The immediate (in the case of this experiment defined up to 5 s) jump as soon as stress is applied (Fig. 2, I).
- Two different cushioned increases with retardation times of 12 and 80 s (Table 2, Fig. 2, II).
- A further viscous increase of strain (Fig. 2, III).

It is hypothesised that the initial, immediate jump in strain involves stretching of the chain fragments of the ALE polymers between crosslinks, such as entanglements and ion (Ca^{2+}) bonds. Since the elastic modulus of polymer networks is proportional to the number density of crosslinks, the increase of the initial modulus with Ca^{2+} concentration (Fig. 5) shows that this ion plays an important role in the network formation. The viscous behaviour in the end of the experiment can be interpreted as a balance between breaking and making of bonds. The whole gel slowly flows. The flow is slower when more Ca^{2+} is available (comparing the slopes of the creep curves in Fig. 7) since the density is higher and more crosslinks need to be broken with increasing strain. The retardation time estimated for those bonds is in the range of 1000 s, in correspondence with earlier findings: for biofilm EPS networks with Ca^{2+} crosslink lifespans of 20–30 min have been found (Ehret and Böl, 2013). It could be related to disentanglement of the ALE (EPS) polymers, which occurs over time scales longer than breaking single crosslink bonds like Ca^{2+} bridges.

The two Kelvin elements describe interactions with a lifespan of around 12 s and 80 s, respectively. An assignment to specific interactions is complicated because of the not yet full characterisation of ALE. Possible candidates are the interactions between Ca^{2+} and the guluronic acid resp. mannuronic acid in ALE (Lin et al., 2013), or between Ca^{2+} and sulphated groups in ALE (Felz et al., 2020). Understanding these interactions on a molecular basis and what effect they have on the mechanical removability, would allow for a more rational search for optimal cleaning agents and doses.

In our previous paper (Pfaff et al., 2021) it was noted that maturing of ALE films leads to a filamentous network with voids that grow over time. This process probably starts already at the microscale in freshly prepared ALE gels, which causes local inhomogeneity. Presumably, it also changes the rheological behaviour. Details on the microscopic structure of the gels can however not be derived from (macroscopic) rheology measurements, so this aspect was not followed up on in the current work.

3.3. Structure breakdown and recovery

Most cleaning strategies against biofouling involve the application of external stress to remove the biofilms. In the following section, the behaviour of the ALE gels towards stresses beyond the breaking point will be discussed. The crossover point (cf. Fig. 5) shifted towards higher stresses and lower strains with increasing calcium concentration (see also Fig. A3, supplementary material). Gels with less Ca^{2+} can deform up to 200% before the structure breaks, while the gels with higher Ca^{2+} content already break at 100% strain.

A special feature was visible at the upper limit of the LVER for the different Ca^{2+} concentrations (Fig. 8): a slight strain stiffening occurred before the breakdown of the structure, indicated by the presence of a maximum in storage modulus. In other words, the structure became harder (less elastic) just before it yielded. This effect became more prominent with increasing Ca^{2+} concentrations. Strain stiffening is a property commonly found in soft biological tissue (Storm et al., 2005) and has been occasionally reported for biofilms (Böl et al., 2013). At this moment it is not possible to differentiate between stiffening due to strain or due to strain rate. The latter could partly be explained by an increase of the contribution of short lifetime bonds (e.g. hydrogen bonds). In this case, extra power is necessary to break bonds, which at lower strain rates would break by themselves. The decrease of the phenomenon with decreasing Ca^{2+} concentration is probably related to the decreasing ALE density (cf.

Fig. 3). The simplest explanation for real strain stiffening would be an accumulation of stretching but not breaking junctions. When the structure eventually breaks, the slope is steeper the more $CaCO_3$ is

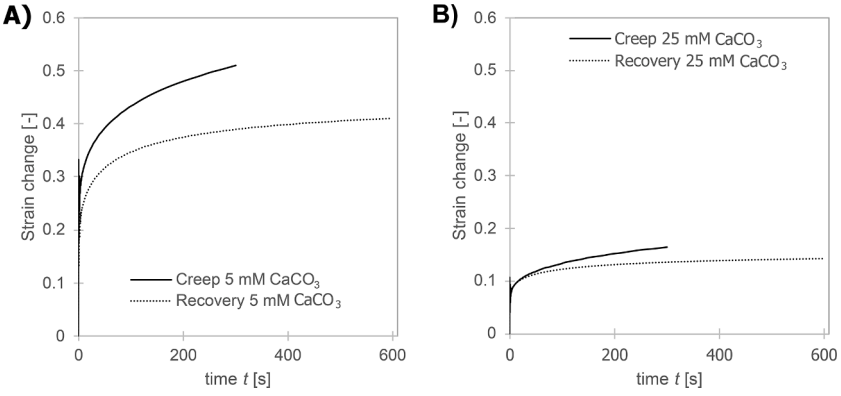

Fig. 7. Comparison of the creep (straight) and recovery (dotted) steps of ALE gels with 5 mm Ca^{2+} (left) and 25 mm Ca^{2+} (right). Absolute values of the changes in strain ε are presented (the changes are positive during creep and negative during recovery steps).

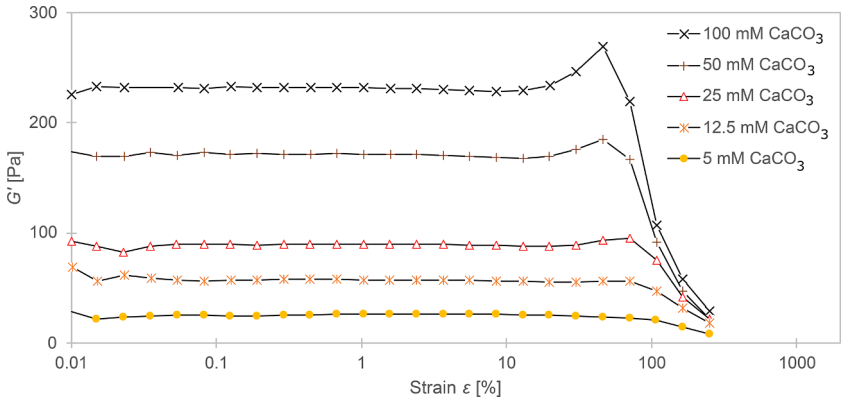

Fig. 8. Set of storage moduli G' of ALE gels with different $CaCO_3$ concentrations as a function of shear strain ε during amplitude sweeps (10 rad/s).

contained in the samples (Fig. 8). Steeper slopes are associated with higher brittleness. Those materials are likely to break into inhomogeneous chunks that are expected to heal poorly. Therefore, recovery from stress might be imperfect. The slighter slope at low $CaCO_3$ concentrations describes a rather ductile deformation (cf. *Error! Reference source not found.*). Such ductile deformation can be expected to allow for better recovery (He et al., 2018).

For a better understanding of the observed strain hardening, breaking and potential recovery of the gels' structure, strain steps were performed. Here, 10, 30 and 200% strain were applied for 120 s each, while in between these steps the relaxing behaviour at 0.3% strain was observed for 400 s. In

Fig. 9, the storage modulus *G'*, loss modulus *G"* and dissipation factor tan *δ* throughout a representative oscillation recovery experiment are presented. A comparison of the behaviour of the storage moduli of the gels with different $CaCO_3$ concentrations is shown in Fig. 10.

The response of the storage modulus *G'* to the application of the different strains was very similar for all $CaCO_3$ concentrations. At 10% strain, only a small decrease compared to the baseline was observed, followed by full recovery. At 30% strain, the storage modulus decreased a bit more than during the 10% strain. Still, all gels kept their predominantly solid behaviour.

A remarkable observation is that the storage moduli during the recovery phase after 30% strain increased to about 120% of their original values (well visible in Fig. 10). This suggests that the strain hardening also observed above (Fig. 8) is caused by changes in the gel's structure that are irreversible on the time scale of the measurements. A possible molecular explanation for this behaviour is that the originally randomly coiled ALE molecules get stretched and aligned under shear, while at the same time crosslinks with lower life-times break and bind again, fixing to some extent the new alignment (Erk et al., 2010). When subsequently a lower shear force is applied, the ALE molecules are already stretched somewhat, and breaking of the weaker bonds does not allow as much stretching as initially, so that the ALE gel appears stiffer than originally. Whether or not this explanation of the strain hardening applies, it is clear that the elastic modulus of the gels depends on the strain history. This memory effect is an important factor considering the common practice of scratching biofilms for investigation.

At 200% strain, eventually, the loss modulus passes the storage modulus, and the gels predominantly behave like liquids (Figs. 9 and 10). As apparent in

Fig. 9, the typically solid behaviour was restored quickly when the strain was reduced again. Within the observation time of 400 s, between 60 and 90% of the original storage moduli were recovered. This distinctive self-healing effect is probably a consequence of the undirected, covalent crosslinks. Once one bond is broken, another one can be quick and easily formed, stabilizing the new conformation. The full original storage modulus could not be reached though, which hints at a permanent destruction of parts of the network. A possible explanation is that ALE molecules were broken during the treatment. The average binding enthalpy of a C—O bond as it is found in the glycosidic linkages of guluronic and mannuronic acid in alginate is 360 kJ/mol (Atkins and Paula, 2006). The maximum shear stress applied during 200% strain was between 50 Pa for ALE gels with 5 mm $CaCO_3$ and towards 200 Pa for 50 and 100 mm $CaCO_3$. With the sample area, defined by the plate radius of 125 mm, and the maximum strain of 200% of 1 mm, the corresponding average transmitted energy on the gels as a whole can be roughly estimated between 50 μJ and 200 μJ. It is not possible to determine which part of this energy is actually available to break the bonds. However, the energy is in a range where breaking of C—O bonds is possible

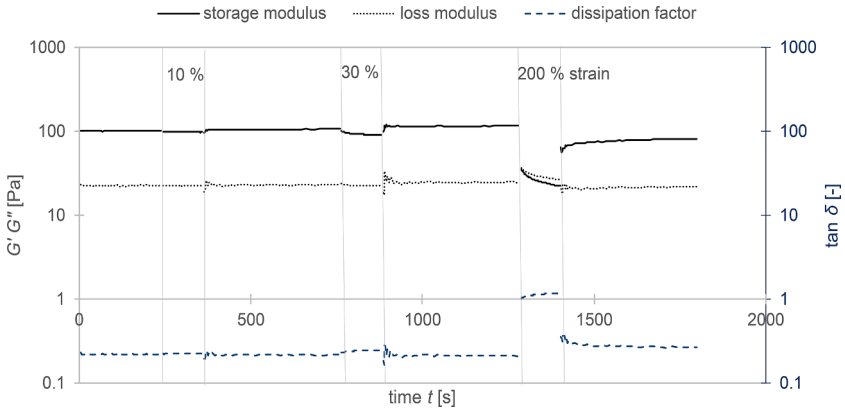

Fig. 9. Typical behaviour of the storage modulus G', loss modulus G" and dissipation factor tan δ in oscillation experiments applying 10, 30 and 200% strain. The baseline and recovery are recorded in the linear viscoelastic region at 0.3% strain. The results depicted are for 40 mg/L ALE, 25 mm $CaCO_3$.

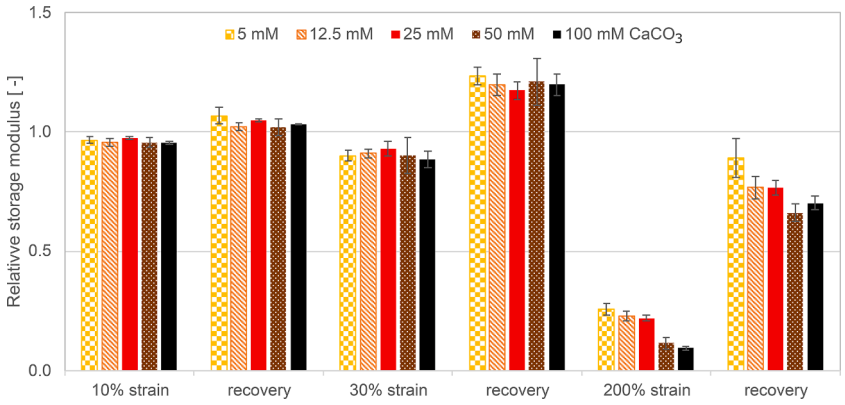

Fig. 10. Relative storage modulus, normalized to the initial storage modulus at 0.3% strain, during the oscillation recovery experiments. The error bars show the standard deviation over the performed triplicates.

(considering the abovementioned binding enthalpy, in principle about 0.3 nmol of C—O bonds could be broken). A slight trend is observed that the gels with high $CaCO_3$ recover less than those with less $CaCO_3$ (Fig. 10). This is in agreement with the higher brittleness of the gels with high $CaCO_3$. The chunks produced upon breaking are more inhomogeneous and therefore recombine less strong than the more flexible structure of the gels with less $CaCO_3$.

The course of the recovery after 200% oscillatory strain is very similar for all tested $CaCO_3$ concentrations. After an initial jump to around 60% recovery, there is a fast increase within the first 15–20 s to ca. 80%, followed by a slower further recovery. We hypothesise that the rather quick recovery in the beginning depicts the elastic response of what is still intact of the network, and the rebuilding of the physical interactions (like electrostatic bonds that are built after slight rearrangement, e.g. by moving of Ca^{2+} ions). The subsequent slow further recovery of the original modulus can have several mechanisms, including further synaeresis, which were not further investigated in this work.

The fast and thorough recovery, even after complete break-down of the crosslinks, emphasises one of the big challenges in biofouling removal. It has been proposed before that mechanical removal of biofilms should be preceded by weakening of the chemical structure (Flemming, 2020). This is supported by our work: as well as mere chemical treatment cannot remove biofouling, neither can simple force, even if it is strong enough to initially overcome the cohesion of the films. A promising approach for the future may even include a series of alternating chemical and physical treatments.

3.4. Outlook

The mechanical properties of gels with relatively low $CaCO_3$ concentrations are in good correspondence with those of real biofilms, which makes the Ca-ALE system a suitable starting model to study biofilm properties in relation to the development of biofouling cleaning methods. A full chemical characterisation of ALE will be useful for assignment of molecular interactions to observed behaviour. Such work could further support the existence of at least two distinguishable interactions with Ca^{2+} involved in the cohesion of Ca-ALE gels. A potential candidate are sulphated groups as they have been identified in ALE (Felz et al., 2020).

The ALE gel model can be extended by adding more ingredients encountered in real biofilms, such as proteins, DNA and (nano) particles.

This work provides a first approach to identify the significant interactions, so that in future applications they can be specifically attacked to facilitate subsequent mechanical removal of biofouling. While this work has focused on understanding the cohesion of ALE gels as a model for biofilms, an additional important field for research for cleaning purposes is the adhesion of biofilms to surfaces.

4. Conclusions

Gels made from bacterial ALE exhibit synaeresis as a function of the calcium content. The more calcium is contained in the gels, the more water is expelled, correlating with stiffer and more brittle gels.

There is an optimum calcium concentration for gelation of ALE, providing suitable mechanical strength without overdosing. The upper limit found in this work is between 1.25 and 2.5 mol/g VSS. Overdosing beyond this limit can promote weakening of the gel structure by precipitation of calcium compounds. Making the ALE network more brittle at the same time and therefore less likely to reconnect can be used as a cleaning approach.

At least three different kinds of crosslinks appear to be present in the investigated calcium-ALE system, with retardation times in the order of 10, 100 and 1000 s.

ALE gels exhibit strain hardening at mid-level strain, illustrating a dependency of the mechanical properties of biofilm samples on their strain history. Therefore, it is questionable how much the analysis of scratched biofilms still can tell about the properties of natural biofilms.

ALE gels show fast and under many conditions quite complete recovery after shear. This emphasises the undirected physical and thus easily recoverable nature of the crosslinks. For successful mechanical cleaning, therefore, the applied force may not be stopped too soon.

Declaration of Competing Interest

The authors declare that they have no known competing financial interests or personal relationships that could have appeared to influence the work reported in this paper.

Acknowledgements

This work was performed in the cooperation framework of Wetsus, European Centre Of Excellence For Sustainable Water Technology (www.wetsus.nl). Wetsus is funded by the Dutch Ministry of Economic Affairs and Ministry of Infrastructure and Environment, the European Union Regional Development Fund, the Province of Fryslân, and the Northern Netherlands Provinces. The authors would like to thank the members of the research theme ``Biofilms'' for fruitful discussions and financial support.

Supplementary materials

Supplementary material associated with this article can be found, in the online version, at doi:10.1016/j.watres.2021.117835.

References

Atkins, P.W., Paula, J.de, 2006. Appendix 4 - Tables. Physikalische Chemie, 4th ed. Wiley-VCH Verlag GmbH & Co. KGaA, Weinheim, pp. 1099–1138.

Böl, M., Ehret, A.E., Bolea Albero, A., Hellriegel, J., Krull, R., 2013. Recent advances in mechanical characterisation of biofilm and their significance for material modelling.', critical reviews in biotechnology. In: Inf. Healthc. N. Y., 33, pp. 145–171. https://doi.org/10.3109/07388551.2012.679250.

Davidovich-Pinhas, M., Bianco-Peled, H., 2010. A Quantitative Analysis of Alginate Swelling', Carbohydrate Polymers, 79. Elsevier, pp. 1020–1027. https://doi.org/10.1016/J.CARBPOL.2009.10.036.

Decho, A.W., Flemming, H., Neu, D.T.R., Wingender, D.J., 2016. Unique and baffling aspects of the matrix: EPS syneresis and glass formation during desication. The Perfect Slime: Microbial Extracellular Polymeric Substances (EPS). IWA Publishing, London, pp. 207–226.

Draget, K.I., Østgaard, K., Smidsrød, O., 1989. Alginate-based solid media for plant tissue culture. Appl. Microbiol. Biotechnol. 31 (1), 79–83. https://doi.org/10.1007/BF00252532.

Ehret, A.E., Böl, M., 2013. Modelling mechanical characteristics of microbial biofilms by network theory. J. R. Soc. Interface R. Soc. 10 (78), 1–12. https://doi.org/10.1098/rsif.2012.0676.

Erk, K.A., Henderson, K.J., Shull, K.R., 2010. Strain stiffening in synthetic and biopolymer networks. Biomacromolecules 11 (5), 1358–1363. https://doi.org/10.1021/bm100136y.

Ewoldt, R.H., Mckinley, G.H., 2007. Creep ringing in Rheometry or how to deal with oft-discarded data in step stress tests. Rheol. Bull.

Felz, S., Al-Zuhairy, S., Aarstad, O.A., van Loosdrecht, M.C.M., Lin, Y.M., 2016. Extraction of structural extracellular polymeric substances from aerobic granular sludge. J. Vis. Exp. (115), e54534. https://doi.org/10.3791/54534.

Felz, S., Neu, T.R., van Loosdrecht, M.C.M., Lin, Y., 2020. Aerobic granular sludge contains Hyaluronic acid-like and sulfated glycosaminoglycans-like polymers. Water Res. 169. https://doi.org/10.1016/j.watres.2019.115291.

Flemming, H.C., 2020. Biofouling and me: my Stockholm syndrome with biofilms. Water Res. 173, 115576 https://doi.org/10.1016/j.watres.2020.115576.

Geesey, G.G., 1982. Microbial exopolymers: ecological and economic considerations. Am. Soc. Microbiol. News 48 (1), 9–14. Available at: https://ci.nii.ac.jp/naid/10017164720/en/.

Ghafoor, A., Hay, I.D., Rehm, B.H.A., 2011. Role of exopolysaccharides in pseudomonas aeruginosa biofilm formation and architecture. In: Appl. Environ. Microbiol. Am. Soc. Microbiol., 77, pp. 5238–5246. https://doi.org/10.1128/AEM.00637-11.

Goode, C., Allen, D.G., 2011. Effect of calcium on moving-bed biofilm reactor biofilms. Water Environ. Res. 83 (3), 220–232. https://doi.org/10.2175/106143010x12780288628255.

Grindy, S.C., Learsch, R., Mozhdehi, D., Cheng, J., Barrett, D.G., Guan, Z., Messersmith, P.B., Holten-Andersen, N., 2015. Control of hierarchical polymer mechanics with bioinspired metal-coordination dynamics. Nat. Mater. 14 (12) https://doi.org/10.1038/nmat4401.

He, Q., Huang, Y., Wang, S., 2018. Hofmeister effect-assisted one step fabrication of ductile and strong gelatin hydrogels. Adv. Funct. Mater. 28 (5) https://doi.org/10.1002/adfm.201705069.

Hermansson, E., Schuster, E., Lindgren, L., Altskär, A., Ström, A., 2016. Impact of solvent quality on the network strength and structure of alginate gels. Carbohydr. Polym. 144, 289–296. https://doi.org/10.1016/j.carbpol.2016.02.069.

International Labour Organization (2009) Calcium gluconate. Available at: http://www.ilo.org/dyn/icsc/showcard.display?p_version=2&p_card_id=1736 (Accessed: 12 February 2020).

International Labour Organization (2012) Calcium carbonate. Available at: http://www.ilo.org/dyn/icsc/showcard.display?p_lang=en&p_card_id=1193&p_version=2 (Accessed: 12 February 2020).

Körstgens, V., Flemming, H.C., Wingender, J., Borchard, W., 2001. Influence of calcium ions on the mechanical properties of a model biofilm of Mucoid pseudomonas aeruginosa. Water Sci. Technol. 43 (6), 49–57. https://doi.org/10.1371/journal.pone.0091935.

Kuo, C.K., Ma, P.X., 2001. Ionically crosslinked alginate hydrogels as scaffolds for tissue engineering: part 1. Structure, gelation rate and mechanical properties. Biomaterials 22 (6), 511–521. https://doi.org/10.1016/S0142-9612(00)00201-5.

Lin, Y.M., Sharma, P.K., van Loosdrecht, M.C.M., 2013. The chemical and mechanical differences between alginate-like exopolysaccharides isolated from aerobic flocculent sludge and aerobic granular sludge. Water Res. 47 (1), 57–65. https://doi.org/10.1016/j.watres.2012.09.017.

Patsios, S.I.I., Goudoulas, T.B.B., Kastrinakis, E.G.G., Nychas, S.G.G., Karabelas, A.J.J., 2015. A novel method for rheological characterization of biofouling layers developing in membrane bioreactors (MBR). J. Memb. Sci. 482, 13–24. https://doi.org/10.1016/j.memsci.2015.02.016.

Pfaff, N.M., Kleijn, J.M., van Loosdrecht, M.C.M., Kemperman, A.J.B., 2021. Formation and ripening of alginate-like exopolymer gel layers during and after membrane filtration. Water Res. 195. https://doi.org/10.1016/j.watres.2021.116959.

Safari, A., Tukovic, Z., Walter, M., Casey, E., Ivankovic, A., 2015. Mechanical properties of a mature biofilm from a wastewater system: from microscale to macroscale level. Biofouling 31 (8), 651–664. https://doi.org/10.1080/08927014.2015.1075981.

Scherer, G.W., 1989. Mechanics of syneresis I. Theory. J. Non Crystal. Solids N.-Holl. 108 (1), 18–27. https://doi.org/10.1016/0022-3093(89)90328-1.

Seviour, T., et al., 2019. Extracellular polymeric substances of biofilms: suffering from an identity crisis. Water Res. Pergamon 151, 1–7. https://doi.org/10.1016/j.watres.2018.11.020.

Storm, C., Pastore, J.J., MacKintosh, F.C., Lubensky, T.C., Janmey, P.A., 2005. Nonlinear elasticity in biological gels. Nature 435 (7039), 191–194. https://doi.org/10.1038/nature03521.

Vinogradov, A.M., Winston, M., Rupp, C.J., Stoodley, P., 2004. Rheology of biofilms formed from the dental plaque pathogen streptococcus mutans. Biofilms 1, 49–56. https://doi.org/10.1017/s1479050503001078.